Evidence for two electronic phases in $Y_{1-x}La_xTiO_3$ from thermoelectric and magnetic susceptibility measurements

H. D. Zhou and J. B. Goodenough
Texas Materials Institute, ETC 9.102, The University of Texas at Austin, 1 University Station, C2201, Austin, Texas 78712, USA
(Received 7 December 2004; revised manuscript received 27 January 2005; published 31 May 2005)

Structural, transport, and magnetic measurements on nearly oxygen stoichiometric samples of the system $Y_{1-x}La_xTiO_3$ and $LuTiO_3$ have revealed that antiferromagnetic $LaTiO_3$ is a *p*-type conductor with holes spread over more than 10 Ti-atom centers in itinerant-electron clusters having a motional enthalpy $\Delta H_m = 0.035$ eV. With the substitution of Y for La, short-range orbital-order fluctuations introduce ferromagnetic interatomic spin-spin interactions that increasingly reduce the magnitude of the Weiss constant θ and suppress T_N as x decreases. The volume fraction of a localized-electron, orbitally ordered second phase containing small-polaron holes increases with decreasing $x < 0.6$ until it becomes the majority phase for $x \leqslant 0.3$ with static orbital ordering below a temperature T^* that increases as x decreases. The volume fraction of the ferromagnetic phase does not reach unity at $x = 0$, but it approaches unity in $LuTiO_3$. Antiferromagnetic interactions across orbital-order antiphase interfaces lowers to zero the remanence of the ferromagnetic phase. The data appear to distinguish an itinerant-electron antiferromagnetism in the La-rich samples from a localized-electron ferromagnetic phase with a cooperative Jahn-Teller distortion.

DOI: 10.1103/PhysRevB.71.184431 PACS number(s): 75.30.Cr, 75.30.Kz, 72.20.Pa, 72.80.Ga

I. INTRODUCTION

Oxygen stoichiometry in the $RTiO_3$ perovskites is difficult to achieve; the best samples commonly have nearly 0.4% excess oxygen, which translates to a rare-earth deficiency of about 0.5% to 1.0% in $R_{1-y}TiO_3$. Since strong electron-electron interactions split the Ti(IV)/Ti(III) and Ti(III)/Ti(II) redox couples by a finite energy gap E_g, the rare-earth deficiency dopes the samples *p*-type by introducing holes into the Ti(IV)/Ti(III) couple. Whereas $LaTiO_3$ is antiferromagnetic below a $T_N = 140$ K with $E_g = 0.2$ eV, $YTiO_3$ is reported to be ferromagnetic below $T_C = 30$ K with an $E_g \approx 1$ eV.[1–3] As the ionic radius of the R^{3+} ion decreases from that of La^{3+}, T_N falls to below 5 K for $R = Sm_{1-x}Gd_x$ and a ferromagnetic T_C, as measured in an applied magnetic field, increases from Gd to Dy.[4] A similar decrease in T_N followed by an increase in T_C with increasing Y concentration in $Y_{1-x}La_xTiO_3$ has also been reported,[1,3] but the evolution of the electronic state with x has not been clarified.

Mizokawa and Fujimori[5] proposed an orbital ordering in $YTiO_3$ to account for the ferromagnetic order following the Goodenough-Kanamori rules for the interatomic spin-spin interactions, and an NMR study by Itoh *et al.*[6] has confirmed this prediction; but no attempt has been made to determine the orbital-ordering temperature T_{OO} and how T_{OO} changes with x in the system $Y_{1-x}La_xTiO_3$. The question of orbital ordering versus an orbital liquid in the other end member $LaTiO_3$ remains controversial,[7–11] but a structural distortion below T_N in $LaTiO_3$ is consistent with a concentration of electronic charge along a [111] octahedral-site axis,[10] which would be consistent with an exchange stabilization associated with type-G antiferromagnetic order. A recent theoretical analysis for $LaTiO_3$ that takes account of the measured temperature dependence of the magnetic susceptibility is consistent with an orbital order that concentrates electronic charge along a [111] octahedral-site axis.[12] Although the molecular-orbital formalism used is appropriate for a strongly correlated electronic system, it does not distinguish between itinerant-electron and localized-electron antiferromagnetism. Since the trigonal crystalline field imparted by the large *A*-site cations in the orthorhombic structure would only increase with the cooperative $TiO_{6/2}$-site rotations on substituting Y for La, the question whether the different orbital order in $LaTiO_3$ and $YTiO_3$ is associated with a change from itinerant to localized strongly correlated electrons remains open.

In this paper, we reexamine experimentally the evolution with x of the transport and magnetic properties of the system $Y_{1-x}La_xTiO_3$ to determine whether there is evidence for itinerant-electron antiferromagnetism in $LaTiO_3$ with a transformation to localized-electron ferromagnetism in $YTiO_3$; such a transformation can be expected to manifest itself by an electronic phase separation accomplished by locally cooperative atomic displacements.[13] We will argue that $LaTiO_3$ is an itinerant-electron antiferromagnet and that a ferromagnetic minority phase increases its volume fraction as $(1-x)$ increases. A zero remanence exhibited by the ferromagnetic phase is interpreted to signal the existence of antiphase boundaries associated with long-range orbital ordering.

II. EXPERIMENT

Polycrystalline samples of $Y_{1-x}La_xTiO_3$ $(0 \leqslant x \leqslant 1)$ and $LuTiO_3$ were prepared by solid-state reactions. Stoichiometric mixtures of $xLa_2O_3 + (1-x)Y_2O_3$ or Lu_2O_3 and Ti_2O_3 were ground together for each composition; the powders were cold pressed into pellets, placed into a molybdenum crucible, and set into a tube that was then evacuated to $\sim 10^{-6}$ torr before firing at 1620 °C for 12 h.

A Perkin-Elmer TGA-7 thermogravimetric analyzer was used to determine the oxygen content of the samples from

TABLE I. Variation with x in $Y_{1-x}La_xTiO_3$ of room-temperature lattice parameters.

X	a (Å)	b (Å)	c (Å)	V(Å^3)
0	5.341(1)	5.686(2)	7.621(1)	231.4
0.1	5.370(1)	5.678(1)	7.658(1)	233.5
0.2	5.401(2)	5.674(1)	7.687(2)	235.6
0.3	5.415(1)	5.668(1)	7.715(1)	236.8
0.4	5.432(1)	5.667(1)	7.728(2)	237.9
0.5	5.451(2)	5.662(1)	7.743(2)	239.0
0.6	5.466(2)	5.660(2)	7.752(1)	239.8
0.65	5.496(2)	5.658(1)	7.791(1)	242.3
0.7	5.528(1)	5.646(2)	7.832(1)	244.5
0.75	5.570(1)	5.633(2)	7.864(1)	246.8
0.8	5.580(1)	5.630(1)	7.901(1)	248.2
0.9	5.608(2)	5.617(1)	7.918(2)	249.4
1	5.633(1)	5.613(2)	7.942(2)	251.1

the weight gain due to an oxidation of the Ti(III) ions to Ti(IV) on heating to 1000 °C in air. For all samples, the excess oxygen was smaller than 0.4%; they were oxygen stoichiometric within experimental error.

Powder x-ray diffraction (XRD) patterns were recorded with a Philips PW 1729 powder x-ray diffractometer equipped with a pyrolytic graphite monochromator and Cu K_α radiation (1.540 59 Å); Si was the internal standard. Data were collected in steps of 0.020° over the range $20° \leqslant \theta \leqslant 60°$ with a count time of 20 s per step. Peak profiles for the XRD data were fitted with the program JADE.

Low-temperature ($5\ \mathrm{K} \leqslant T \leqslant 300\ \mathrm{K}$) magnetic-susceptibility measurements were made on heating with a Quantum Design dc SQUID magnetometer after cooling in zero field (ZFC) or after cooling in a measuring field (FC) of 1 kOe. M-H hysteresis loops of magnetization M versus applied magnetic field H were measured over the range $-5\ \mathrm{T} \leqslant H \leqslant 5\ \mathrm{T}$ at 5 K. High-temperature magnetic-susceptibility ($300\ \mathrm{K} \leqslant T \leqslant 680\ \mathrm{K}$) was measured in $H=5$ T under a pure He atmosphere.

The low-temperature thermoelectric power $\alpha(T)$ was obtained from 80 K to 320 K with a laboratory-built apparatus as described elsewhere.[14] The resistivity was measured by a four-probe technique on samples that were cold pressed as mixed powders. The cold-pressing technique has been described elsewhere.[15] The high-temperature ($320\ \mathrm{K} \leqslant T \leqslant 600\ \mathrm{K}$) thermoelectric power and resistivity were measured in a vacuum of 10^{-5} torr.

III. RESULTS

Room-temperature lattice parameters and unit-cell volumes for the orthorhombic *Pbnm* perovskite system $Y_{1-x}La_xTiO_3$ are given in Table I. All samples were single-phase to XRD. Figure 1 shows that the unit-cell volume varies linearly with x in accordance with Végard's law, but with a break and change of slope near $x=0.7$. Goral *et al.*[1] also reported this break in their study of $Y_{1-x}La_xTiO_3$. Our

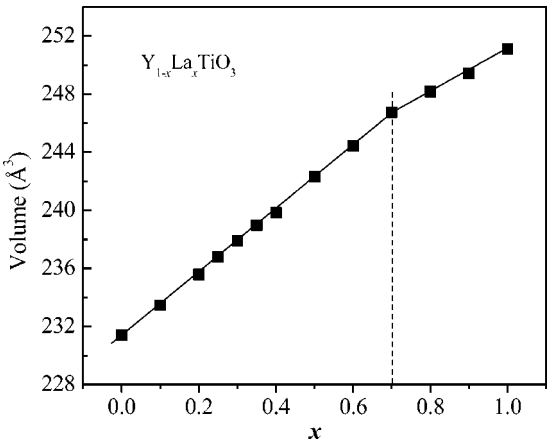

FIG. 1. Room-temperature volume versus x for $Y_{1-x}La_xTiO_3$ ($0 \leqslant x \leqslant 1.0$).

$LuTiO_3$ sample had room-temperature lattice parameters $a=5.275(1)$ Å, $b=5.644(2)$ Å, and $c=7.851(2)$ Å.

Figure 2 shows the temperature dependence of the resistivity $\rho(T)$ for $YTiO_3$ and $LaTiO_3$. At room temperature, the resistivity of $YTiO_3$ is two orders of magnitude larger than that of $LaTiO_3$. A $\rho(T) \sim \exp(-E_a/kT)$ fit for $YTiO_3$ gives an activation energy $E_a \approx 0.25$ eV; the same fit for $LaTiO_3$ applies only in the range $T > 55$ K with an $E_a \approx 0.035$ eV.

Figure 3 shows the temperature dependence of the thermoelectric power $\alpha(T)$ for several compositions of the $Y_{1-x}La_xTiO_3$ system. As x increases from $x=0$ to $x=1.0$, $\alpha(T)$ decreases and becomes nearly temperature independent above 160 K by $x=1.0$. A step decrease in the room-temperature value occurs between $x=0.7$ and $x=0.8$. For $x \leqslant 0.7$, $\alpha(T)$ varies as a semiconductor. For $YTiO_3$, $\alpha(T) \sim \Delta/2kT$ gives a charge-carrier trapping energy $\Delta = 0.14$ eV.

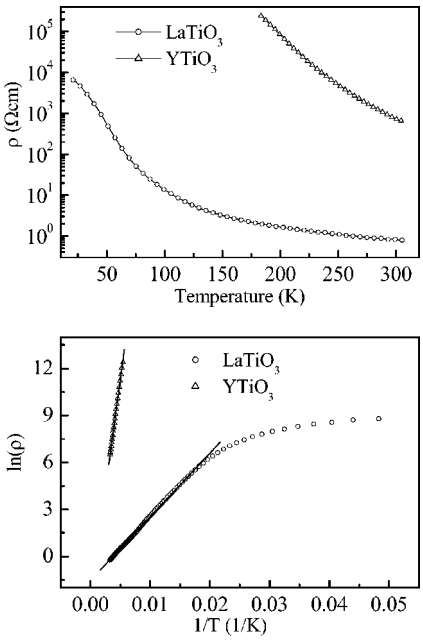

FIG. 2. Temperature dependence below room temperature of resistivity ρ and the $\ln \rho \sim 1/T$ curve for $YTiO_3$ and $LaTiO_3$.

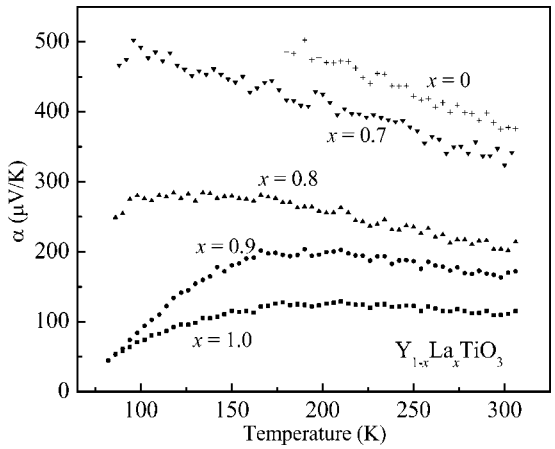

FIG. 3. Temperature dependence of thermoelectric power α for several values of x in $Y_{1-x}La_xTiO_3$.

Figures 4–6 and Table II show the evolution with x of the magnetic properties of $Y_{1-x}La_xTiO_3$. Three compositional ranges can be distinguished, $0 \leqslant x \leqslant 0.3$, $0.35 \leqslant x \leqslant 0.7$, and $0.8 \leqslant x \leqslant 1.0$. In the range $0 \leqslant x \leqslant 0.3$, the paramagnetic susceptibility taken in 1 kOe shows the onset of ferromagnetism below a T_C that decreases linearly with x from 30 K for $YTiO_3$ to below 5 K for $Y_{0.7}La_{0.3}TiO_3$ as determined by the temperature where the inverse molar susceptibility $1/\chi_m(T)$ becomes flat in Fig. 4. However, the M-H curves taken at 5 K exhibit nearly zero remanence for all $0 \leqslant x \leqslant 0.3$ samples and a magnetization at 50 kOe that decreases from 0.8 μ_B/f.u. for $YTiO_3$ to under $0.2\mu_B$/f.u. at $x=0.3$. In order to increase the bending of the Ti-O-Ti bonds beyond that of $YTiO_3$ while keeping the A-site cation nonmagnetic, we investigated the magnetic properties of $LuTiO_3$; the results, given in Fig. 7, show an increase in T_C to 40 K with a Weiss constant $\theta > T_C$ and a magnetization in 50 kOe of nearly $0.9\mu_B$/f.u. However, the M-H loop of $LuTiO_3$ retains a zero remanence.

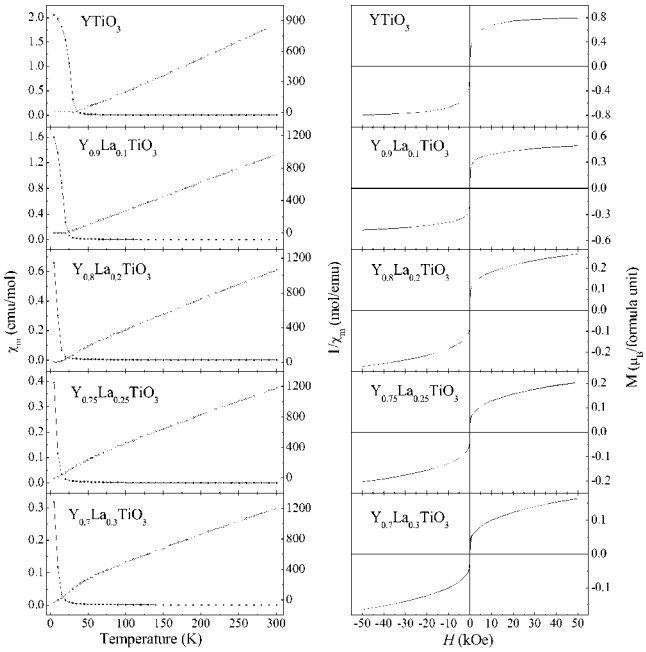

FIG. 4. Temperature dependence below room temperature of the molar magnetic susceptibility χ_m, inverse $1/\chi_m$, measured with $H=1$ kOe, and M-H curves for $Y_{1-x}La_xTiO_3$ at $T=5$ K ($0 \leqslant x \leqslant 0.3$).

Figure 8 shows high-temperature resistivity $\rho(T)$ and thermoelectric-power $\alpha(T)$ data for $YTiO_3$; changes in slopes in the Arrhenius plots occur near 490 K. With $\rho(T) \sim \exp(-E_a/kT)$ and $\alpha(T) \sim \Delta/2kT$, the activation and trapping energies E_a and Δ change, respectively, from 0.18 eV and 0.10 eV above 490 K to 0.25 eV and 0.14 eV below 490 K. The high-temperature ($300\ \text{K} \leqslant T \leqslant 680$ K) paramagnetic susceptibilities of Fig. 9 show a change in the slope of $1/\chi_m(T)$ at T^*; this is the same temperature at which a second-order orbital order-disorder transition has been observed.[6] T^* decreases from 490 K to 450 K to 380 K to just below 300 K for $x=0$, 0.1, 0.2, and 0.3. Figure 10 shows a T^* for $LuTiO_3$ like that in $YTiO_3$. The high-temperature ($T > T^*$) Curie-Weiss law has a Weiss constant $\theta < 0$ for all x that approaches zero for $x=0$.

In the range $0.35 \leqslant x \leqslant 0.7$, the M-H curves develop a hysteresis loop. As x increases, the coercivity H_C increases and the magnetization M at 50 kOe decreases. Moreover, the inverse molar paramagnetic susceptibility exhibits a Curie-Weiss temperature dependence that gives a μ_{eff} and a $|\theta|$ that increase linearly with x, see Fig. 11. An increase with x in the long-range magnetic ordering temperature in the range $0.35 \leqslant x \leqslant 1.0$ contrasts with the decrease in T_C in the range $0 \leqslant x \leqslant 0.3$, so we label this ordering temperature T_N to signal a predominantly antiferromagnetic volume fraction with a weak canted-spin ferromagnetic moment as in $LaTiO_3$.

Figure 11 shows a step increase in H_C at $x \approx 0.7$, the composition where Fig. 1 shows a discontinuity in the slope of volume versus x. For $x > 0.7$, the $1/\chi_m(T)$ curve retains a linear dependence on T, but the μ_{eff} and a $|\theta| > 600$ K obtained by fitting to a Curie-Weiss law increases even more strongly with x to values that are clearly inconsistent with a homogeneous localized-electron model. However, the Néel temperature T_N changes smoothly through this compositional range.

IV. DISCUSSION

A. Transport properties

Although all samples were single-phase to XRD, they were slightly oxidized. Since the structure does not accommodate oxygen interstitials, it must have cation vacancies. The R^{3+} ions are more mobile than the Ti^{3+} ions in these perovskites; therefore, we assume the oxidized compositions correspond to $R_{1-y}TiO_3 + (y/2)R_2O_3$ with $y < 0.01$; the R^{3+}-ion vacancies introduce holes into a Ti(IV)/Ti(III) redox couple that is split from the Ti(III)/Ti(II) couple by an energy gap that increases from $E_g \approx 0.2$ eV in $LaTiO_3$ to 1.0 eV in $YTiO_3$. With this model, the p-type conduction, Fig. 3, is polaronic with a motional enthalpy $\Delta H_m = E_a - (\Delta/2)$; $\Delta H_m = 0.035$ eV in $LaTiO_3$ increases with x to $\Delta H_m = 0.18$ eV in $YTiO_3$.

The resistivities we measured for our samples, Fig. 2, are somewhat higher than those reported by Okada *et al.*[16] for a

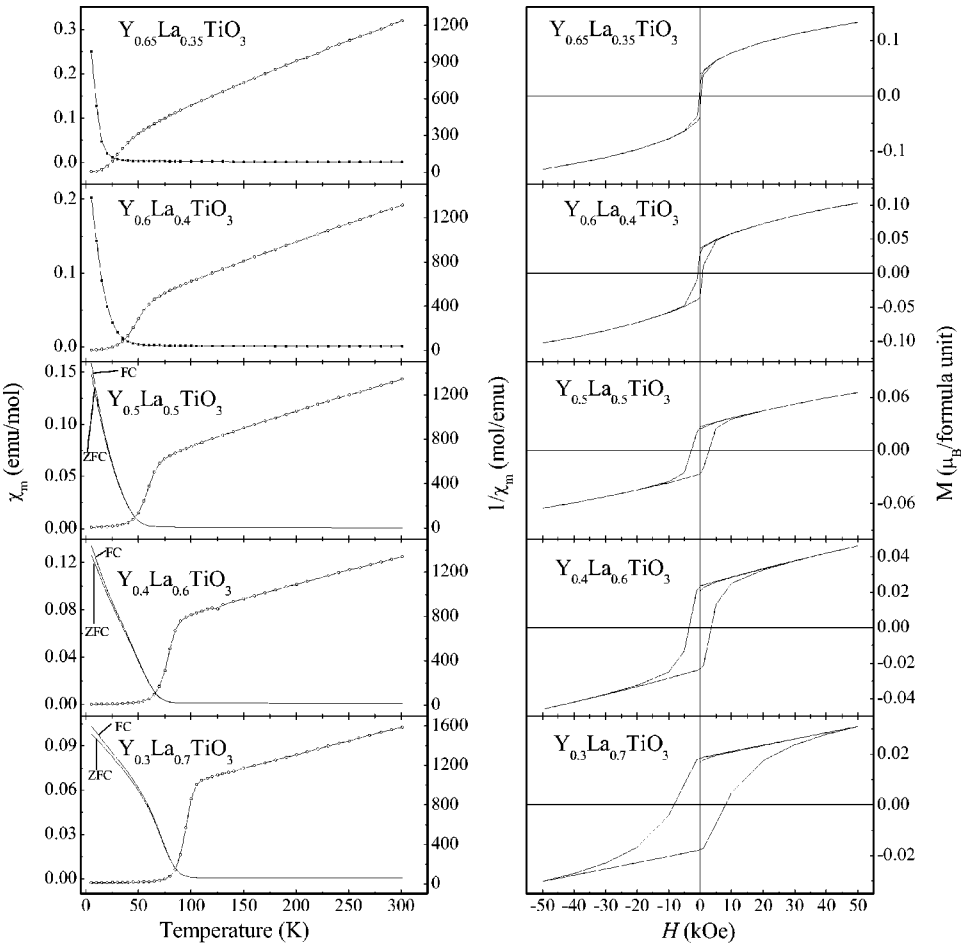

FIG. 5. Temperature dependence below room temperature of the molar magnetic susceptibility χ_m, inverse $1/\chi_m$, measured with $H=1$ kOe, and M-H curves for $Y_{1-x}La_xTiO_3$ at $T=5$ K $0.35 \leqslant x \leqslant 0.7$).

$LaTiO_{3.01}$ crystal, but at low temperature they are nearly seven orders of magnitude lower than those reported by Hemberger *et al.*[10] The oxygen excess in our sample was comparable to that found by Okada *et al.* for their crystal; it corresponds to $c \approx 0.02$ hole/Ti atom. The markedly contrasting low-temperature $\rho(T)$ values reported therefore signal not only that Hemberger *et al.* had an essentially oxygen-stoichiometric crystal, but also that the mobilities of the few holes introduced by a slight oxidation of $LaTiO_3$ must be high.

Where there is no trapping of charge carriers ($\Delta=0$), the thermoelectric power generated by polarons is normally

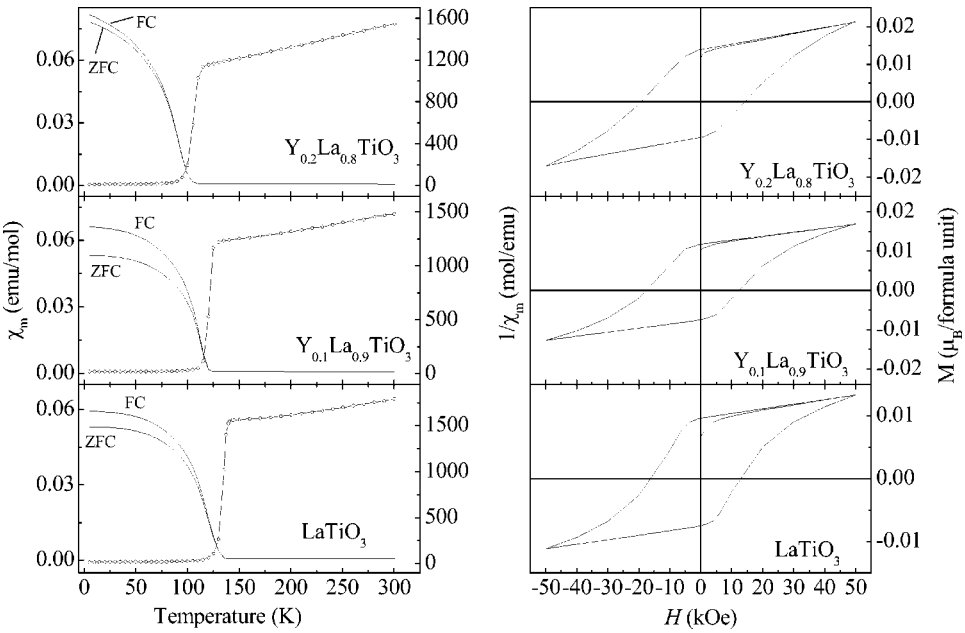

FIG. 6. Temperature dependence below room temperature of the molar magnetic susceptibility χ_m, inverse $1/\chi_m$, measured with $H=1$ kOe, and M-H curves for $Y_{1-x}La_xTiO_3$ at $T=5$ K ($0.8 \leqslant x \leqslant 1.0$).

TABLE II. Magnetic data, including T_C, T_N, coercivity H_C, and calculated parameters μ_{eff} and Weiss constant θ from a linear temperature dependence of $1/\chi_m(T)$ for $Y_{1-x}La_xTiO_3$ and $LuTiO_3$. The μ_{eff} and θ were obtained from high-temperature measurements in $H=50$ kOe.

x	T_C(K)	T_N(K)	H_C (kOe)	μ_{eff} (μ_B/f.u.)	θ (K)
0	30		0	1.80 ($T>490$ K)	−50 ($T>490$ K)
				1.62 ($T<490$ K)	52 ($T<490$ K)
0.1	20		0	1.87 ($T>450$ K)	−104 ($T>450$ K)
				1.73 ($T<450$ K)	−28 ($T<450$ K)
0.2	10		0.007	1.89 ($T>380$ K)	−161 ($T>380$ K)
				1.77 ($T<380$ K)	−93 ($T<380$ K)
0.25	5		0.01		
0.3	0	0	0.057	1.96	−224
0.35		20	0.27		
0.4		40	0.82	2.00	−283
0.5		48	2.78	2.06	−363
0.6		76	3.43	2.11	−415
0.7		93	8.38	2.15	−479
0.8		106	17.2	2.29	−633
0.9		124	17.2	2.34	−726
1		140	17.0	2.43	−853
$LuTiO_3$	40		0	1.79 ($T>500$ K)	−45 ($T>500$ K)
				1.60 ($T<500$ K)	58 ($T<500$ K)

dominated by the temperature-independent statistical component

$$\alpha_s = (k/e)\ln[\beta(1-Qc)/Qc], \tag{1}$$

where k is the Boltzmann constant, e is the charge carried by the mobile polarons, $\beta=2$ is the spin-degeneracy factor, c is the fraction of Ti atoms that are Ti(IV), and Q is the number of Ti atoms contained in a mobile polaron. For $LaTiO_3$, with $c\approx 0.03$, which is its upper limit within experimental error, Eq. (1) gives a $Q\approx 10$. Such a large polaron size signals that the polarons are hole-rich itinerant-electron clusters in a strongly correlated matrix. Large clusters would not be trapped by isolated R^{3+}-ion vacancies, which is consistent with a $\Delta=0$. The clusters would be defined by cooperative oxygen-atom displacements at the boundary, and these displacements are significantly smaller than those that define a small ($Q=1$) polaron.[17] Therefore, the motional enthalpy of

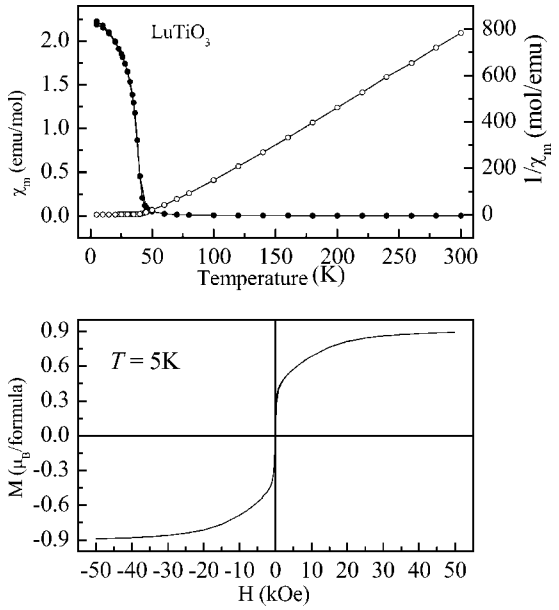

FIG. 7. Temperature dependence below room temperature of the molar magnetic susceptibility χ_m, inverse $1/\chi_m$, measured with $H=1$ kOe, and M-H curve for $LuTiO_3$ at $T=5$ K.

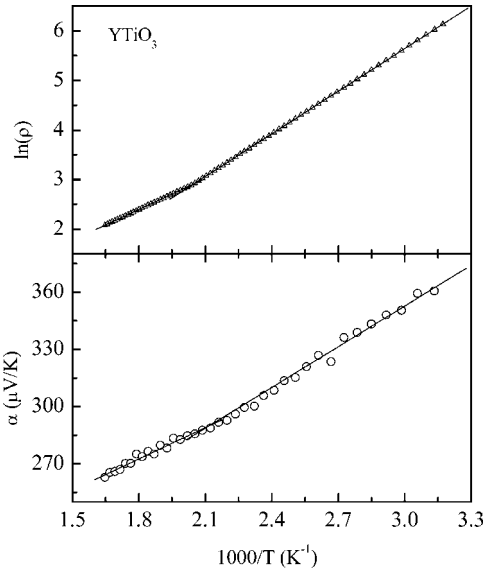

FIG. 8. ln $\rho\sim 1/T$ and $\alpha\sim 1/T$ curves with 300 K$<T<$600 K for $YTiO_3$.

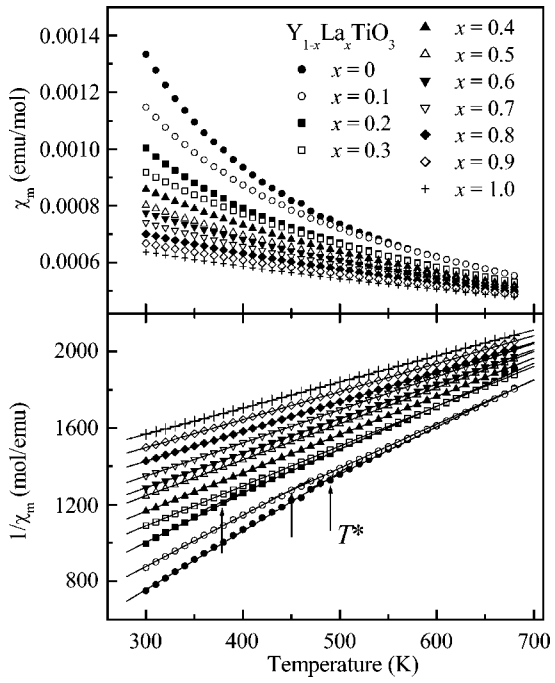

FIG. 9. Temperature dependence above room temperature of molar magnetic susceptibility χ_m and their inverse $1/\chi_m$ for $Y_{1-x}La_xTiO_3$ ($0 \leqslant x \leqslant 1.0$), measured with $H=50$ kOe.

the polaron is small. These data suggest that $LaTiO_3$ may be an itinerant-electron antiferromagnet; it contains strongly correlated, but itinerant π^* electrons.

On the other hand, the *G*-type orbital order responsible for ferromagnetic interactions in $YTiO_3$ signals that the Ti-3*d* electron in the ferromagnetic phase is localized, as does the appearance of a trapping of smaller polarons in $YTiO_3$. From the virial theorem, it has been argued[13] that the equilibrium (M-O) bond is longer for more localized electrons than that for itinerant electrons and that the transition from localized to itinerant electronic behavior is first order. It is the first-order character of the transition that supports a hole-rich itinerant-electron phase as large-polaron clusters in a strongly correlated Ti(III) matrix. As the bandwidth of the

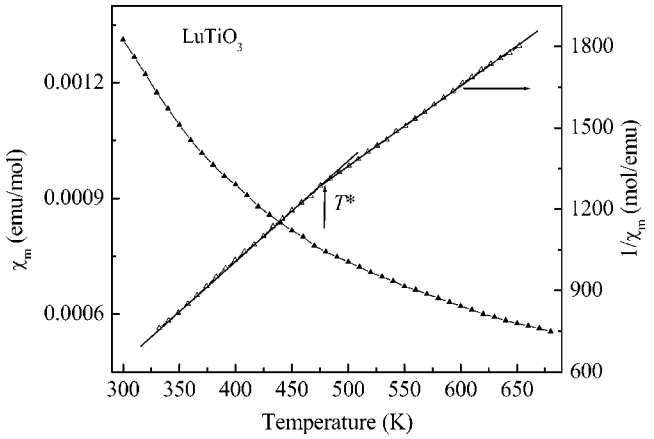

FIG. 10. Temperature dependence above room temperature of molar magnetic susceptibility χ_m and their inverse $1/\chi_m$ for $LuTiO_3$ measured with $H=50$ kOe.

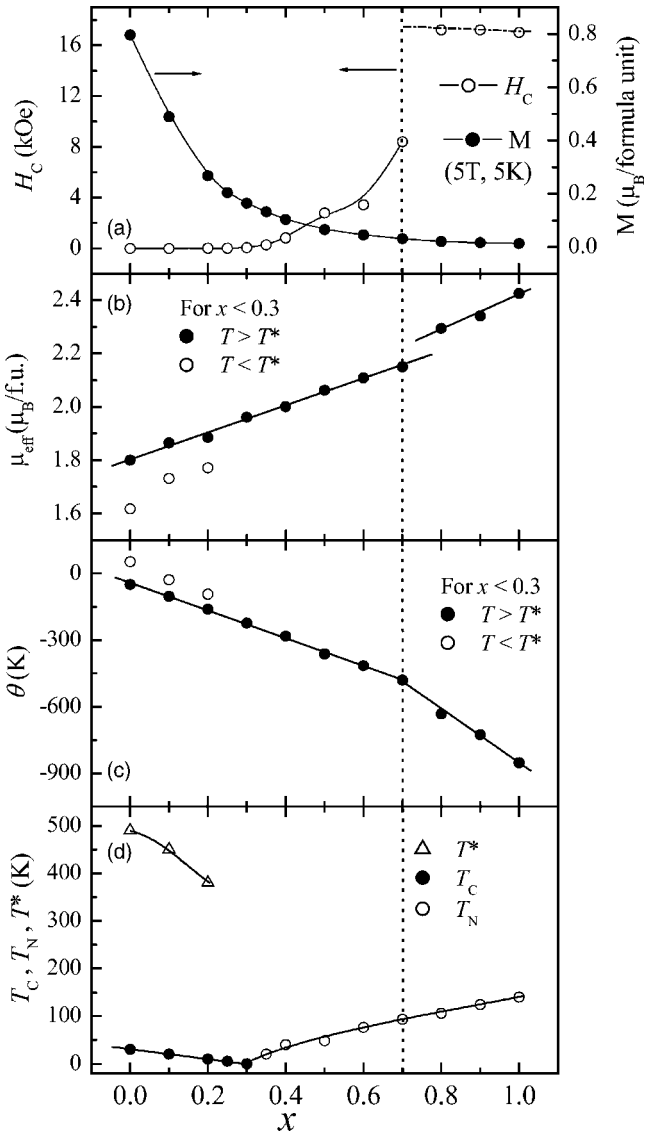

FIG. 11. Magnetic data for $Y_{1-x}La_xTiO_3$, including the variation with x of (a) coercivity H_C and magnetization ($T=5$ K, $H=50$ kOe), (b) μ_{eff}, (c) Weiss constant θ, for $x<0.3$ samples, open circles are obtained with $T<T^*$, and solid circles are obtained with $T>T^*$, (d) T_C, T_N, and T^*. Here μ_{eff} and θ are obtained from the high-temperature measurements in $H=50$ kOe.

matrix redox couple decreases with decreasing x, the polaron size decreases, approaching that of a small polaron in a localized-electron matrix. More problematic is the question whether a transition from itinerant-electron antiferromagnetism to localized-electron, orbitally ordered ferromagnetism is also first order. We now argue that our data support a two-magnetic-phase compositional range for the TiO_3 matrix, thus supporting a first-order phase change between the antiferromagnetic and ferromagnetic regimes.

First, however, we must consider whether to ascribe the change in slope of the volume vs x curve of Fig. 1 to the onset of localized-electron behavior below $x=0.8$. This change of slope is opposite to that we should expect from electronic changes since the equilibrium (Ti-O) bond is longer for localized than itinerant electrons. Therefore, we

conclude that it is due to a change from cooperative rotations of undistorted $TiO_{6/2}$ octahedra at $x \leqslant 0.7$ to octahedral-site distortions superimposed on the cooperative site rotations because of *R*-O interactions that arise where the mean size of the rare-earth ion, as calculated for ninefold oxygen coordination, gives a tolerance factor $t > 0.87$; in the $RFeO_3$ family this tolerance factor is reached at an R^{3+} ionic radius of 1.11 Å.[18]

B. Magnetic evidence for two electronic phases

1. Paramagnetic data

The paramagnetic data reflect the character of the TiO_3 array. In the paramagnetic state where the occupied orbital fluctuates ($T > T^*$ for $0 \leqslant x \leqslant 0.3$, the $\chi_m(T)$ data of Fig. 9 signal antiferromagnetic interatomic spin-spin interactions ($\theta < 0$); the magnitude of the Weiss constant θ decreases linearly to near zero and μ_{eff} approaches the spin-only value as the La content *x* decreases to $x = 0$ through the range $0 \leqslant x \leqslant 0.7$. It thus appears that at $T > T^*$ where the orbitals are disordered, the entire compositional range may be characterized as a single paramagnetic phase in which the exchange interactions change continuously with *x*. In the range $0.7 < x \leqslant 1.0$, the calculated μ_{eff} and θ values of Table II, which appear to be physically unmeaningful, are consistent with a volume fraction of strong-correlation fluctuations within a matrix exhibiting an enhanced Pauli paramagnetism that increases with decreasing *x*. However, at temperatures $T < T^*$ where long-range orbital ordering occurs in the interval $0 \leqslant x \leqslant 0.2$, a $\theta > 0$ in $YTiO_3$ changes to a $\theta < 0$ with increasing *x*; and for $x > 0$, $1/\chi_m(T)$ decreases from the Curie-Weiss linear curve as the temperature is lowered towards T_C and it decreases more strongly with increasing *x*. The shape of the $1/\chi_m(T)$ curve is similar to that of a ferrimagnet, but the orthorhombic perovskite structure does not contain two unequal spin sublattices coupled antiparallel to one another. Rather, the $1/\chi_m(T)$ curves signal the appearance of antiferromagnetic fluctuations, pairs or clusters, within a paramagnetic matrix. Figure 4 shows that this phenomenon increases and the ferromagnetic saturation magnetization decreases with increasing $x \leqslant 0.5$, which signals that the magnetic transition is not global; the volume fraction of an antiferromagnetic second phase having a weak, canted-spin ferromagnetic component increases with *x* until it percolates for $x > 0.3$ and occupies the entire volume for $x > 0.6$. The splitting of the FC and ZFC curves at lower temperatures for $x > 0.4$ samples correlates with the presence of a canted-spin antiferromagnetic phase.

There are two possible driving forces for a phase separation; one is a segregation of the two types of orbital order, each type associated with a cooperative Jahn-Teller distortion, and the other is the first-order character of a transition from localized to itinerant 3*d* electrons. The transport data show that the antiferromagnetic phase would contain mobile holes in "bags" enclosing several Ti atoms whereas the ferromagnetic phase would contain small-polaron holes. Therefore, we believe the orbital order of the ferromagnetic phase is a conventional Jahn-Teller orbital ordering of localized electrons whereas that of the antiferromagnetic phase reflects an optimization of the interatomic Ti-O-Ti interactions for strongly correlated itinerant electrons in an orthorhombic lattice. As *x* decreases below $x = 0.3$, the volume fraction of the localized-electron phase becomes large enough to percolate so as to give long-range orbital order below T^* within a fraction of the volume that becomes ferromagnetic below T_C.

2. M-H data

Samples $0.8 \leqslant x \leqslant 1.0$ of Fig. 6 exhibit a weak ferromagnetic behavior typical of a global canted-spin antiferromagnet. On the other hand, samples $0 \leqslant x \leqslant 0.3$ of Fig. 4 show a ferromagnetic behavior that has no remanence; there is no opening of the *M-H* hysteresis loop and the magnetization at 5 K in 50 kOe never attains the spin-only value of 1 μ_B/f.u. although it increases progressively with decreasing *x* and approaches the spin-only value in $LuTiO_3$. The lack of any remanence even though the magnetization *M* approaches saturation by 20 kOe can only mean that in zero field the ferromagnetic regions become coupled antiparallel to one another. The large magnetization of a ferromagnetic region provides a sufficient torque in a moderate applied magnetic field to align the ferromagnetic regions in opposition to an antiferromagnetic exchange field across the interface between them. However, on removal of the applied field, the antiferromagnetic interactions across an interface boundary realigns the ferromagnetic regions antiparallel to one another.

The origin of this behavior resides in the nature of the orbital order below T^* that gives rise to the ferromagnetic spin-spin interactions. The *G*-type orbital order, which suppresses the orbital angular momentum, has been predicted[5] and identified.[6] Nucleation and growth of many regions of *G*-type orbital order must introduce antiphase boundaries at many interfaces where these regions meet, and the coupling across an antiphase boundary would be antiferromagnetic according to the Goodenough-Kanamori rules for spin-spin interactions. Therefore, we conclude that the lack of remanence signals antiferromagnetic coupling across antiphase boundaries at the interface of orbitally ordered, ferromagnetic regions. A similar phenomenon has been observed in double perovskites where there is atomic rather than orbital ordering.[19]

In the range $0.4 \leqslant x \leqslant 0.6$, any orbital ordering only occurs below room temperature; the dominant phase is antiferromagnetic below T_N with a weak canted-spin ferromagnetism.

V. CONCLUSIONS

$LaTiO_3$ is an itinerant-electron antiferromagnet with no ordering of the threefold-degenerate π-bonding electrons in the paramagnetic phase even though strong correlations split the Ti(IV)/Ti(III) redox couple from the Ti(III)/Ti(II) couple by an energy gap $E_g = 0.2$ eV. Holes introduced by La^{3+}-ion vacancies are spread over more than 10 Ti sites in an itinerant-electron cluster. Substitution of Y for La in $Y_{1-x}La_xTiO_3$ ($0.3 < x < 0.7$) introduces orbital-order fluctuations in the paramagnetic phase that create ferromagnetic spin-spin interactions that progressively reduce T_N of the majority phase as the volume fraction of short-range orbital ordering increases. A change in the variation of lattice volume

with x near $x=0.7$, Fig. 1, is interpreted to signal the introduction of a $TiO_{6/2}$ site distortion superimposed on a cooperative site rotation for $x>0.7$. In the range $0\leqslant x\leqslant 0.3$, orbital ordering below a T^* occurs in a majority phase that becomes ferromagnetic below T_C; both T^* and T_C increases as the volume fraction of the majority phase increases with decreasing x. However, the volume fraction does not reach unity at $x=0$; only in $LuTiO_3$ does it approach unity. The ferromagnetic phase exhibits a zero remanence because of antiferromagnetic coupling across antiphase boundaries at the interface of regions with out-of-phase orbital ordering.

ACKNOWLEDGMENTS

The NSF and the Robert A. Welch Foundation of Houston, TX, are thanked for financial support.

[1] J. P. Goral, J. E. Greedan, and D. A. MacLean, J. Solid State Chem. **43**, 244 (1982);J. P. Goral and J. E. Greedan, J. Magn. Magn. Mater. **37**, 315 (1983).
[2] J. D. Garrett, J. E. Greedan, and D. A. Maclean, Mater. Res. Bull. **16**, 145 (1981).
[3] Y. Okimoto, T. Katsufuji, Y. Okada, T. Arima, and Y. Tokura, Phys. Rev. B **51**, 9581 (1995).
[4] J. E. Greedan, J. Less-Common Met. **111**, 335 (1985);G. Amow, J.-S. Zhou, and J. B. Goodenough, J. Solid State Chem. **154**, 619 (2000).
[5] T. Mizokawa and A. Fujimori, Phys. Rev. B **51**, R12880 (1995); **54**, 5368 (1996).
[6] M. Itoh, M. Tsuchiya, H. Tanaka, and K. Motoya, J. Phys. Soc. Jpn. **68**, 2783 (1999).
[7] B. Keimer, D. Casa, A. Ivanov, J. W. Lynn, M. v. Zimmermann, J. P. Hill, D. Gibbs, Y. Taguchi, and Y. Tokura, Phys. Rev. Lett. **85**, 3946 (2000).
[8] G. Khaliullin and S. Maekawa, Phys. Rev. Lett. **85**, 3950 (2000).
[9] K. Kikoin, O. Entin-Wohlman, V. Fleurov, and A. Aharony, J. Magn. Magn. Mater. **272-276**, 346 (2004).
[10] J. Hemberger, H. A. Krug von Nidda, V. Fritsch, J. Deisenhofer, S. Lobina, T. Rudolf, P. Lunkenheimer, F. Lichtenberg, A. Loidl, D. Bruns, and B. Büchner, Phys. Rev. Lett. **91**, 066403 (2003).
[11] V. Fritsch, J. Hemberger, M. V. Eremin, H.-A. Krug von Nidda, F. Lichtenberg, R. Wehn, and A. Loidl, Phys. Rev. B **65**, 212405 (2002).
[12] R. M. Eremina, M. V. Eremin, S. V. Iglamov, J. Hemberger, H.-A. Krug von Nidda, F. Lichtenberg, and A. Loidl, Phys. Rev. B **70**, 224428 (2004).
[13] J. B. Goodenough, Struct. Bonding (Berlin) **98**, 1 (2001).
[14] J. B. Goodenough, J.-S. Zhou, and J. Chan, Phys. Rev. B **47**, 5275 (1993).
[15] J.-S. Zhou, J. B. Goodenough, and B. Dabrowski, Phys. Rev. B **67**, 020404(R) (2003).
[16] Y. Okada, T. Arima, Y. Tokura, C. Murayama, and N. Möri, Phys. Rev. B **48**, 9677 (1993).
[17] G. I. Bersuker and J. B. Goodenough, Physica C **274**, 267 (1997).
[18] J.-S. Zhou, J. B. Goodenough, and B. Dabrowski (unpublished);M. Marezio and P. D. Dernier, Mater. Res. Bull. **6**, 23 (1971);M. Marezio, J. P. Remeika, and P. D. Dernier, Acta Crystallogr., Sect. B: Struct. Crystallogr. Cryst. Chem. **B26**, 2008 (1970).
[19] H. Q. Yin, J.-S. Zhou, R. Dass, J.-P. Zhou, J. T. McDevitt, and J B. Goodenough, J. Appl. Phys. **87**, 6761 (2000);J. B. Goodenough and R. I. Dass, Int. J. Inorg. Mater. **2**, 3 (2000).